Journal of Materials Chemistry A

Accepted Manuscript

ROYAL SOCIETY OF CHEMISTRY

www.rsc.org/materialsA

Journal of Material Chemistry A

PAPER

Hierarchical nanoparticles-induced superhydrophilic and under-water superoleophobic Cu foam with ultrahigh water permeability for effective oil/water separation

Received 00th January 20xx,
Accepted 00th January 20xx

DOI: 10.1039/x0xx00000x

www.rsc.org/

Zhi-Yong Luo, Kai-Xuan Chen, Jun-Hui Wang, Dong-Chuan Mo* and Shu-Shen Lyu*

In recent years, Cu foam has attracted intensive attention owing to its remarkable performance for oil/water separation. Most research mainly focused on Cu foam with surfactant decoration, which results in superhydrophobic or even stimuli-responsed membranes. Fabricating Cu foam with intrinsic superhydrophilicity via simple operations still remains as a challenge. Herein, we synthesized superhydrophilic and under-water superoleophobic Cu foam that consists of oxy-chloridized hierarchical nanoparticles with metal Cu core and polar $Cu_2O/CuO_{1-x/2}Cl_x$ shell via the combination of anodization, HCl etching and calcination. This material shows ultrahigh water permeability (5 μl water-droplet permeating within 9 ms). And the oil/water separation efficiency of superhydrophilic Cu foam (SCuF) is above 99% with the oil content in separated water lower than 3 ppm. Moreover, the oil/water separation performance of SCuF for repeated use and anti-corrosion are also excellent. To the best of our knowledge, it is the first attempt to synthesize intrinsic superhydrophilic Cu foam for effective oil/water separation. Due to the greatly enhanced specific surface area and active sites, it has potential applications in catalysis, hydrogen evolution process, electrode materials and many other environmental protection and energy fields.

1. Introduction

Metal foam, one of significant functional materials, has attracted intensive attentions in recent years, which is mainly due to their remarkable virtues such as ultralow density,[1, 2] high specific surface area,[3] open-pore structures,[4] high strength-to-weight ratio, excellent electrical conductivity[5] and so on. This kind of material has extensive applications in energy system,[3] catalysis,[6] sensor,[7] oil/water separation,[5, 8, 9] etc..

Up to now, research mainly focused on Au,[10] Ni,[11] Cu,[12-14] Ti[9, 15] foams and even alloy foams[16] due to the combination of excellent properties and mature processing techniques,[2, 17, 18] among which Cu foam has received more attentions recently. For instances, Dong et al.[19] reported a three-dimensional Cu foam coated by Cu_2O nanothorn arrays for efficient nonenzymatic detection of glucose in 2015; Li and his co-workers[20] had a similar research, in which the Cu foam was decorated by CuO nanowires and exhibited high sensitivity for glucose mainly due to its high electrical conductivity and specific surface area. Owing to the porosity and stability, Cu foam had been regarded as a template for the design of novel materials, such as graphene-like copper oxide nanofilms,[21] metal-organic framework-5,[14] 3D-graphene network,[22] electrodes,[12, 23] and so on. Besides, Cu foam also shows enormous potential in the field of heat transfer[24] and removal of heavy metal ions.[25, 26]

Oil/water separation faces severe challenges due to the frequent crude oil spill accidents and the increasing amount of industrial wastewater. In contrast to traditional membrane separation, gravity-driven oil/water separation is more efficient, either flux or energy-cost, among which superhydrophilic membranes possess superior advantages like anti-pollution, easier recycle etc.. Decorating metal mesh via hydrophilic components like hydrogel,[27] surfactant,[28] copper,[29] $Cu(OH)_2$,[30] palygorskite,[31] titanium dioxides,[32, 33] tungsten oxide,[34] zeolite,[35] nickel,[36] etc. is the main idea to design superhydrophilic membranes. Although excellent oil/water separation performance is obtained, it will be faces enormous issues in real world applications. For examples, hydrogel is easy to swell and becomes soft when hydrated,[37] thus results in degenerated efficiency; the mechanical strength of mesh coated by hydrophilic inorganics is insufficient for industrial application, which is mainly due to the poor adhesive force between inorganics and mesh. Cu foam is an ideal matrix for gravity-driven oil/water separation because of appropriate mechanical strength and porosity.

School of Chemical Engineering and Technology, Sun Yat-sen University, Guangzhou 510275, China. E-mail: modongch@mail.sysu.edu.cn and lvshsh@mail.sysu.edu.cn; Fax: +86-020-84112150

Electronic supplementary information (ESI) available: Fig. S1 – S2: XPS analysis of surface Cu species after anodization and after HCl etching. Fig. S3: XPS analysis of surface Cl species after HCl etching. Fig. S4: O 1s spectrum of anodized Cu foam before and after storing. Fig. S5 – S6: droplet tests and oil/water separation performance of anodized Cu foam. Fig. S7: morphologies of SCuF after immersing in corrosive solutions. See DOI: 10.1039/b000000x

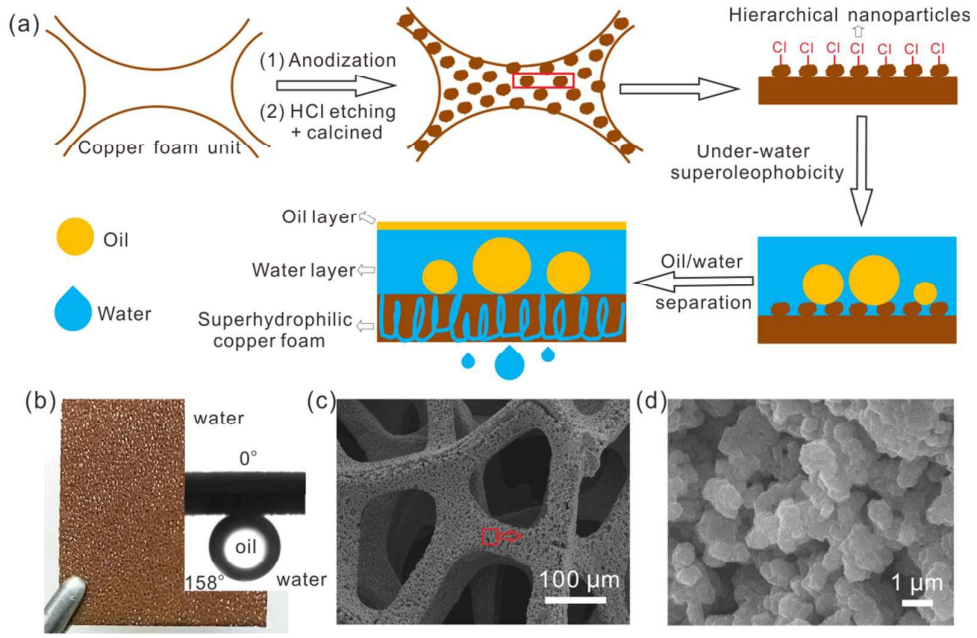

Scheme 1 (a) Schematic of the fabrication of superhydrophilic Cu foam (SCuF) and its application for oil/water separation. (b) the photograph of specimen, the inset-photographs are the water contact angle in air and the under-water oil contact angle, respectively. the droplet is 5 μl. (c) the SEM image of the prepared Cu foam. (d) the surface morphology of the Cu foam unit.

Cu foam via appropriate modification exhibits excellent performance for gravity-driven oil/water separation or oil collection. To date, research was mainly focused on superhydrophobic Cu foam[13, 38, 39] decorated by low-surface-energy surfactants or appropriate nanostructures, but this kind of Cu foam is easy fouled by adhered or adsorbed oils and difficult to recycle. Superhydrophilic Cu foam shows superior advantages for oil/water separation when compared to the superhydrophobic ones, but there is few attention on this aspect. In 2015, Lin et al.[5] demonstrated an electricity-induced switchable surface of an N-dodecyltrimethoxysilane modified Cu foam for a controllable oil/water separation process under a low-voltage load, which is the first time to utilize the superhydrophilicity of Cu foam for oil/water separation for all I know. However, the process from superhydrophobicity to superhydrophilicity of Cu foam relies on the impressed voltage. Fabricating Cu foam with intrinsic superhydrophilicity via simple operations still remains as a challenge and greatly encouraged.

Herein, we synthesized, for the first time, superhydrophilic Cu foam (SCuF) for effective oil/water separation. This SCuF is composed of oxy-chloridized hierarchical nanoparticles with metal Cu core and $Cu_2O/CuO_{1-x/2}Cl_x$ shell via the combination of anodization, HCl etching and calcination, the Cl-terminated groups were formed at the surface of Cu-NPs in the form of -O-Cu-Cl or even -Cu-Cl (see Scheme 1). This SCuF shows ultrahigh water permeability and remarkable oil/water separation performance (separation efficiency > 99%). We also demonstrated the properties of SCuF for repeated use and anti-corrosion. On account of the surface hierarchical nanoparticles, this SCuF owns greatly enhanced specific surface area than that of the previous reports, leading to lots of applications like catalysis, elctrode materials, etc.. It also can bear much more scratch or friction cycles than those meshes coated by superhydrophilic substances due to its layer-by-layer structure, thus results in potential possibility for real world applications.

2. Experimental section

2.1 Materials and methods

Before anodization, Cu foam (purity ≥ 99.5%, size 3 cm × 3 cm, thickness 1 mm) was cleaned in acetone, ethanol and deionized water in ultrasonic cleaner (50 KHZ), respectively, and then immersed in 10 vol% H_2SO_4 to remove the oxide layer and dried. Anodization was carried out on a two-electrode electrochemical cell[40] in which used Cu foam as anode and a piece of copper foil (purity ≥ 99.7%, size 3 cm × 3 cm) as the cathode, the distance between the two electrodes was 1.5 cm. The electrolyte consists of 0.1 wt% NH_4F and 99.9 wt% H_2O. The bath temperature was kept at 25 °C.

Cu foam was anodization for 2 h and dried in air atmosphere. Then etched for 20 min by using 1 M HCl under the stiring condition of 300 r/min. At last, the specimen was calcined at 200 °C for 3 h under air atmosphere.

2.2 Material characterization

The morphology of the specimens was characterized by a scanning electron microscope (SEM, JSM-6510LV) and a transmission electron microscope (TEM, FEI Tecnai G2 F30). The components of the specimens were analyzed by energy

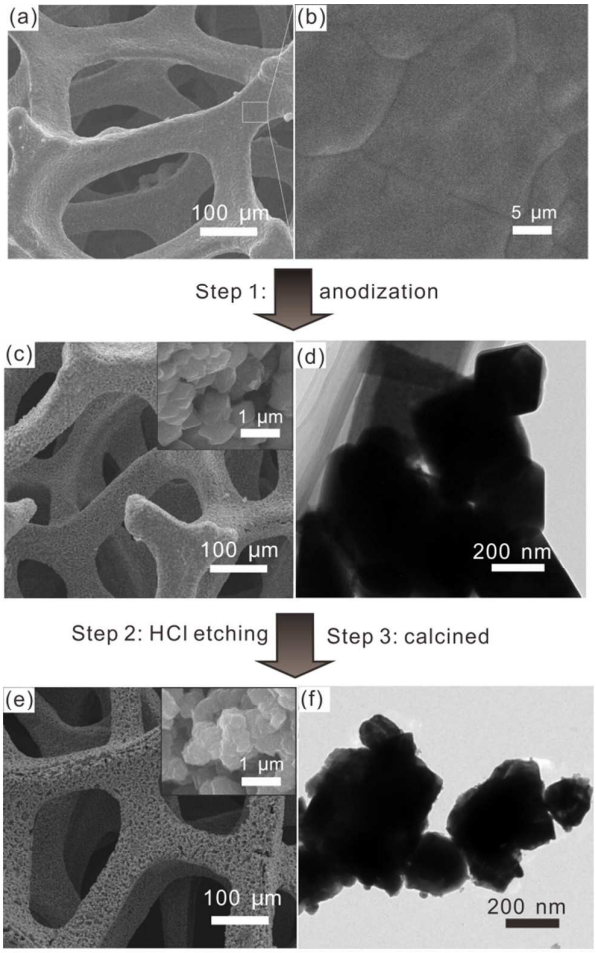

Fig. 1 SEM and TEM characterization of Cu foam. SEM image of (a) original specimen; (b) surface morphology of Cu foam unit; (c) specimen after anodization and (e) final specimen, respectively. The inset-photographs of (c) and (e) are the surface morphologies of specimens. (d) and (f) are the TEM characterization of nanoparticles corresponding to specimen (c) and (e).

dispersive spectrometer (EDS) and X-ray photoelectron spectrum (XPS, ESCALab250). The crystal form was confirmed via an X-ray diffractometer (XRD, Empyrean).

The contact angle and dynamic effect of 5 μl deionized water droplet spreading out on the interfaces was carried out via a high-speed camera (Vision Research Phantom V.211 capturing at 3000 frames per second). The under-water oil contact angle and slide angle of 5 μl oil was captured via a high-speed camera (Vision Research Phantom V.211 capturing at 100 frames per second) and accessary adjusting bracket, the under-water adhesive test was carried out via a PTFE tube to manipulate the oil droplet.

2.3 Oil/water separation

In this section, hexane, iso-octane, petroleum ether (three kinds of saturated oils), paraxylene (a kind of unsaturated oil) and diesel (a kind of mineral oil), five kinds of selected oils, were applied for oil/water separation. The SCuF were placed

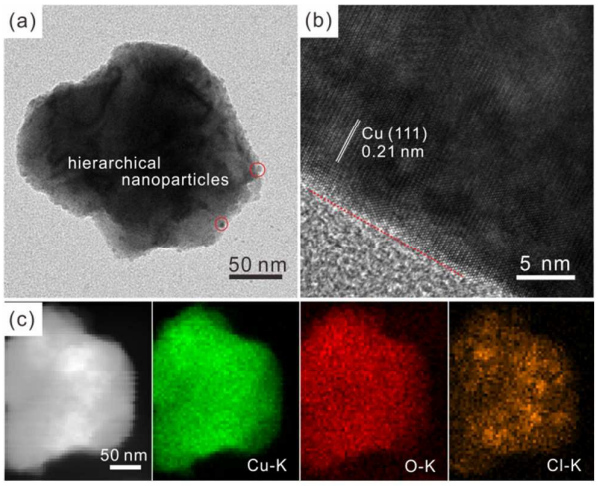

Fig. 2 TEM characterization of Cu-NP. (a) TEM image of hierarchical Cu-NP. (b) the HR-TEM analysis of Cu-NP. (c) STEM and corresponding element mapping of Cu, O and Cl.

between two quartz tubes (d = 2 cm) with flange, and fastened via screws.

The oil/water mixture (water/oil = 10) was separated from the upper tube to the lower tube. After separation, the water (60 ml) was acidized (PH = 1 to 2) via 1M HCl and added 2g NaCl to demulsify (according to the operations of instrument). Then it was extracted twice by using 40 ml CCl_4. The extractant was dried by anhydrous Na_2SO_4. The oil content of original oil/water mixture and separated water were measured via an infrared oil content analyzer (OIL-8, China). The copper/cuprous ion concentration in corrosive solution was analysed via a PE plasma atomic emission spectrometer (AES, Optima 8300).

3. Results and discussion

3.1 Characterization of materials

Fig. 1 shows the transformation of morphology and structure of Cu foam during the processes. As shown in Fig. 1a-b, Cu foam is made up of a large amount of Cu foam units (see schematic 1a) and micro-pores, the pore diameter is 100 - 300 μm. The surface of Cu foam unit consists of crystal boundary and it is smooth relatively. After anodization, the surface of Cu foam is turned into rough and consists of Cu nanoparticles (Cu-NPs)[5] (see Fig. 1c). Fig. 1d shows the TEM image of Cu-NP that exhibits polygonal appearance with clear facets, which may be mainly due to the exsitence of fluorine.[41, 42] The size of Cu-NP varies from 200 to 500 nm.

Then the specimen was treated via 1 M HCl etching and calcined at 200 °C for 3h. From Fig. 1e, we can see the Cu foam unit turned into poly-porous structue owing to the corrosivity of HCl, the pore is composed of nanoparticles (see inset-photograph of Fig. 1e). The Cu-NP shows an irregular appearance, and the shell of Cu-NP turned into rough.

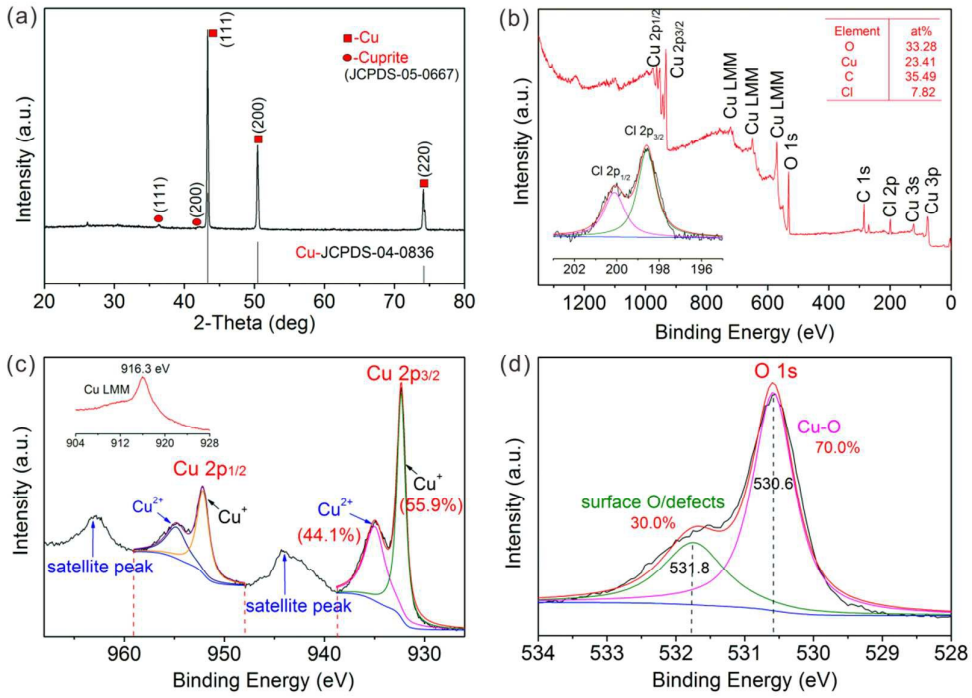

Fig. 3 The XRD and XPS characterization of SCuF. (a) the XRD analysis of SCuF. (b) the full-spectrum, (c) Cu 2p and (d) O 1s spectrum of XPS analysis. The inset-photographs of (b) and (c) are Cl 2p and Cu LMM of XPS analysis, respectively.

As shown in Fig. 2a, the Cu-NP is covered by smaller nanoparticles (see red circle in Fig. 2a), which exhibits hierarchical structure. Fig. 2b shows the the high resolution TEM (HR-TEM) photograph of Cu-NP, it is noticed that the lattice parameter in core is 0.21 nm, the typical value of Cu (111) (JCPDS-04-0836), meaning that the subject of Cu-NP is metal Cu. Fig. 2c shows the elements mapping of Cu, O and Cl, three kinds of elements. Cu distributes evenly on the whole area of Cu-NP, which agrees with the HR-TEM results that the subject of Cu-NP is metal Cu. Meanwhile, The foreign oxygen and surface Cl species, originating from the surface oxidation (or even hydro-oxidation) during electrodeposition and HCl etching, respectively, are mainly distributes on the surface of Cu-NP. Therefore, the signal intensity of O and Cl are weaker than Cu relatively, especially the Cl. This Cu foam which is formed by hierarchical nanoparticles exhibits remarkable superhydrophicity and under-water superoleophobicity shown in Scheme 1b.

Wettability of solid interfaces is mainly dependent on its surface energy and roughness.[43, 44] In order to make clear the surface components of the Cu-NP, we analyzed the specimen by using XRD and XPS. As shown in Fig. 3a, the specimen is composed of metal Cu and cuprite (a form of Cu_2O),[45, 46] which is in agreement with the values in the standard cards (JCPDS-04-0836 and JCPDS-05-0667), respectively. The peaks of cuprite is weak, meaning that the cuprite content of Cu-NP is very low.

XPS characterization shows that the surfaces of Cu-NP is composed of 33.28 at% O, 23.41 at% Cu, 7.82 at% Cl and 35.49 at% C, four kinds of elements (see Fig. 3b). From the inset-photograph of Fig. 3b, we can see the Cl 2p peak is split into Cl $2p_{3/2}$ peak at 198.5 eV and Cl $2p_{1/2}$ peak at 200.2 eV, which is the typical values of Cl-terminated group reported in the previous work.[47] this Cl-terminated group may be in the form of surface -O-Cu-Cl or even -Cu-Cl, which is in favour of the formation of superhydrophilic interface.[48-50] Fig. 3c shows the XPS analysis of Cu 2p, the Cu $2p_{3/2}$ is split into two peaks at 932.5 eV and 935 eV, respectively, combining with Cu LMM at 916.3 eV,[51] the peak at 932.5 eV is related to Cu^+ of Cu_2O.[51, 52] Meanwhile, the peak at 935 eV is related to surface Cu^{2+},[53] especially copper oxy-chloride or copper chloride ($CuO_{1-x/2}Cl_x$). The ratio of Cu^+ and Cu^{2+} is 55.9% and 44.1%, respectively. The peaks of Cu $2p_{1/2}$ at 952.5 eV and 955 eV are the corresponding values for Cu^+ and Cu^{2+}, respectively. The Cu-NP consists of metal Cu core and $Cu_2O/CuO_{1-x/2}Cl_x$ shell.

What's more, we analyzed the surface oxygen species. The O 1s is split into two peaks at 530.6 eV and 531.8 eV, which are attributed to Cu-O bonds of cuprous oxide and absorded O species (hydroxyl, H_2O et al.) or even defects, respectively.[54, 55] The surface O species of Cu-NPs are composed of 70% Cu_2O and 30% absorbed oxygen species/defects, which also benefits the formation of SCuF.

Further, in order to demonstrate the formation of superhydrophilic Cu-NPs, especially the $Cu_2O/CuO_{1-x/2}Cl_x$ shell, we analyzed the surface components via XPS during the preparation. First of all, the Cu foam was treated by anodization in fluorine-containing electrolyte, the reactions taken place at anode as following equation (1) and (2):

$$Cu \rightarrow Cu^{2+} + 2e^- \quad (1)$$

$$2Cu + H_2O \rightarrow Cu_2O + 2H^+ + 2e^- \quad (2)$$

The Cu foam was dissolved partly and the surface of Cu-NP was oxidized into Cu_2O on account of the limited oxygen content in the electrolyte. As shown in Fig. S1, the Cu_2O is confirmed via the combination of Cu 2p and Cu LMM peak, the ratio of Cu_2O is 94.5%, aparting from 5.5% CuO which is generated from the further oxidation of Cu_2O in air. Meanwhile, the facets of Cu-NPs were exposed due to the existence of fluorine,[42, 56] showing a polygonal appearance (see Fig. 1d). Then, the specimen was prepared via HCl etching, the reactions proceeded as following equation (3) and (4):

$$Cu_2O + 2H^+ \rightarrow 2Cu^+ + H_2O \quad (3)$$

$$Cu_2O + xCl^- + xH^+ \rightarrow Cu_2O_{1-x/2}Cl_x + (x/2)H_2O \quad (4)$$

After HCl etching, the surface Cu_2O was dissolved slightly as reaction (3) went on, which results in the destruction of clear facets of Cu-NPs (see Fig. 1d and 1f). What's more, the Cl^- reacted with Cu_2O and generated $Cu_2O_{1-x/2}Cl_x$ as reaction (4) went on. Fig. S2 shows the XPS analysis of surface Cu species after HCl etching, only Cu^+ was confirmed at 932.5 eV and 952.5 eV, Cu LMM peak at 916.4 eV is related to the typical value of Cu_2O. At the same time, Cl-terminated groups were confirmed in Fig. S3. The Cl-terminated groups, in the form of $Cu_2O_{1-x/2}Cl_x$, were generated due to the replacement of lattice oxygen by Cl^- partly.[57] Therefore, the Cu^+ shown in Fig. S2 is the combination of Cu_2O and $Cu_2O_{1-x/2}Cl_x$.

$$4Cu_2O_{1-x/2}Cl_x + O_2 \rightarrow 4CuO_{1-x/2}Cl_x + 2Cu_2O \quad (5)$$

At last, the specimen was calcined under air atmosphere. On one hand, the Cl-teminated compounds turned into $CuO_{1-x/2}Cl_x$ due to the oxidation process in air atmosphere (eq. 5), in which the Cu^+ were oxidized into Cu^{2+}. On the other hand, the rest of Cu^+ in $Cu_2O_{1-x/2}Cl_x$ were existed in the form of Cu_2O due to the replacement of Cl by O, which is in agreement with the above results shown in Fig. 3c. It is worth noting that the Cu^{2+} shown in Fig. 3c is almost related to Cu species in $CuO_{1-x/2}Cl_x$. Therefore, the superhydrophilic Cu-NPs composed of metal Cu core and $Cu_2O/CuO_{1-x/2}Cl_x$ shell is synthesized, showing excellent superhydrophilic properties on account of the polar $Cu_2O/CuO_{1-x/2}Cl_x$ shell.

3.2 Droplet experiments

Droplet tests are the fundament of interfacial applications, especially oil/water separation.[27, 30] As shown in Fig. 4a, the water-droplet that coloured by methylene blue permeated on Cu foam, the original one shows hydrophobicity, while the anodized one and SCuF own excellent superhydrophilicity. However, after storing in normal laboratory environment for 3 months, the wettability of anodized Cu foam was degenerated may be owing to the removal of surface polar components like absorbed water and surface –OH (see Fig. S4). Fortunately, the SCuF owns stable superhydrophilicity, which is mainly due to

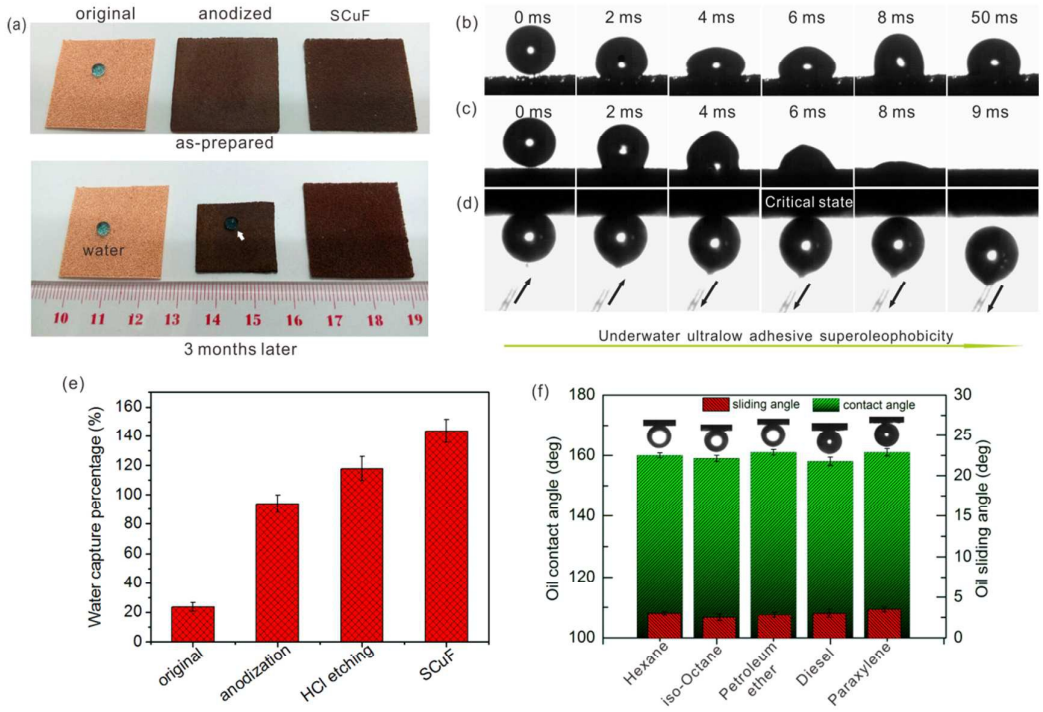

Fig. 4 Droplet tests of SCuF. (a) the visual tests of water droplet wetting Cu foam. High-speed dynamic images of 5 μl water droplet spreading out on Cu foam (b) before and (c) after treatment. (d) the under-water oil adhesive effect of SCuF, the oil model is paraxylene. (e) the water capture percentage of Cu foam before treatment, after anodization, after HCl etching and the final SCuF. (f) the under-water oil contact angles and sliding angles, the oil droplet is 5 μl.

its polar $Cu_2O/CuO_{1-x/2}Cl_x$ shell. Fig. 4b shows the high-speed dynamic water droplet spreading out on original Cu foam, the water contact angle is about 110 degrees, exhibiting hydrophobic property as well as unsuitability for oil/water separation. The SCuF shows ultrahigh water permeability, for which 5μl water droplet permeated within 9 ms (see Fig. 4c). According to the previous works, 3 – 5 μl water droplet permeated through superhydrophilic porous menbranes within 28 – 280 ms.[30, 32, 58, 59] The water permeability of SCuF is significant higher than the former reported values. It is worth noting that the ultrahigh water permeability is mainly due to the superhydrophilic hierarchical Cu-NPs with metal Cu core and $Cu_2O/CuO_{1-x/2}Cl_x$ shell. Moreover, the under-water oil adhesive test was carried out in Fig. 4d, which shows under-water superoleophobicity and ultralow adhesion force. It benefits the excellent oil/water separation performance.

It has been reported that the trapped water serves as a repulsive liquid phase for oils to contact with the membrane directly,[30] thus results in more oleophobic interfaces as more water is captured. Fig. 4e shows the water capture percentage (WCP) of Cu foam during the preparation, the amount of captured water is enhanced as the formation processes go on. The WCP of SCuF is up to around 145%, which is also in favour of efficient oil/water separation.

The original Cu foam shows hydrophobicity, which may be on account of surface oxidation or absorption of carbon species in air. The WCP is about 20%. After anodization, the Cu foam unit turned into Cu-NPs with clear facets (see Fig. 1c-d), resulting in hydrophilic foam with higher specific surface area. The WCP is about 90%. Then superhydrophilic Cu-NPs with metal Cu core and $Cu_2O/Cu_2O_{1-x/2}Cl_x$ shell is generated after HCl etching, which is mainly owing to the superhydrophilic Cl-terminated compounds and hierarchical nanostructures, the WCP is up to 120%. What's more, we calcined the Cu foam at 200 °C, by which the $Cu_2O/CuO_{1-x/2}Cl_x$ shell, the surface nanostructures and defects were generated, thus results in a more hydrophilic material. Therefore, the aim of the steps of preparation is to elevate the wettability, specific surface area or even active cites for oil/water separation. It is proved to be effective.

Under-water oil contact angle (OCA) and oil sliding angle (OSA) are two crucial factors affecting oil/water separation

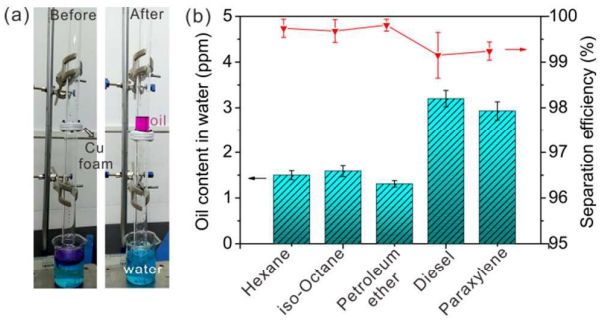

Fig. 5 The oil/water separation performance. (a) the photographs of oil/water separation performance of Cu foam before and after treatment. (b) the oil content in separated water and the corresponding separation efficiency.

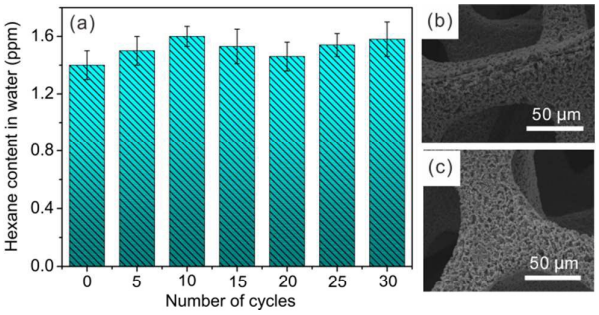

Fig. 6 (a) The properties of SCuF for repeated use. The SEM images (b) before and (c) after repeated use.

performance. A larger OCA and smaller OSA, meaning that the oil droplet can easily roll off the surface and the oil-adhesion of the surface is extremely low, are conducive to efficient oil/water separation. From Fig. 4f, this SCuF shows large OCA (155° - 160°) combining with small OSA (3° - 4°). The state of the oil droplet can be described by the Cassie model,[60] and the contact angle can be expressed as formula (6):

$$\cos\Theta'_{OCA} = f\cos\Theta_{OCA} + f - 1 \qquad (6)$$

where Θ'_{OCA} and Θ_{OCA} are the under-water oil contact angle on the rough surface and flat surface, respectively, f is the area fraction of the solid, which is defined as the ratio of the actual contact area by the oil droplet to the whole area of the SCuF.[31] Specifically, in the present work, Θ_{OCA} = 112°, Θ'_{OCA} = 158° for hexane, so f = 0.12, meaning that about 90% of the contact area is the oil/water contact interface. Therefore, the under-water superoleophobic and easily rolling performances can be observed, which is in favour of the formation of membranes for oil/water separation with excellent performance.[29]

3.3 Oil/water separation

In this section, we demonstrated the oil/water separation performance, the repeated use and anti-corrosive properties of ScuF for oil/water separation.

3.3.1 Oil/water separation of SCuF

Fig. 5a shows the visual photographs of oil/water separation. As we can see, the oil/water separation performance of SCuF is well in contrast to the original one. Specifically, the oil content in separated water is below 1.5 ppm (see Fig. 5b) for hexane, iso-octane and petroleum ether, three kinds of saturated oils, which is mainly due to the weak interaction force between carbon chains of oils and water layer. The paraxylene content in separated water is about 3 ppm, higher than the saturated oils, which is mainly owing to the relative stronger interaction force between the π electron of paraxylene and protonated H of water molecules, agreeing with Lewis's theory of valency. In particular, the oil/water separation performance for diesel is inferior to the others relatively, which may be on account of relative hydrophilic impurities in it. All in all, the the oil content in separated water is below 3 ppm.

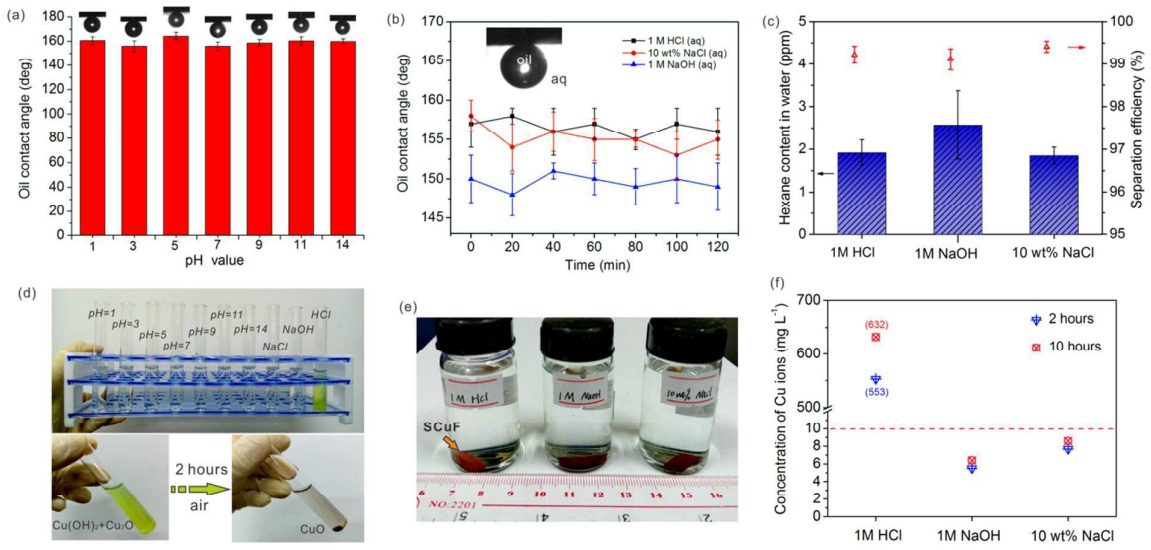

Fig. 7 The anti-corrosive properties of SCuF. (a) the under-water oil contact angles (OCA) under varied pH values. (b) the relationship between OCA and immersed time in 1 M HCl, 10 wt% NaCl and 1 M NaOH solution, respectively. The oil model is paraxylene. (c) the performance of SCuF for oil/corrosive solution separation. (d) the precipitation reactions of solution after SCuF immersed for 2 h. (e) The samples of 50 mg SCuF immersed in 20 ml corrosive solution. (f) the Cu ion concentration in corrosive solution, the solution was obtained as shown in (e).

Moreover, we provided the separation efficiency in Fig. 5b, in which the separation efficiency was calculated by oil rejection coefficient (R(%)) according to formula (7):[27]

$$R(\%) = (1 - C_p/C_o) \times 100 \qquad (7)$$

where C_o and C_p are the oil concentration of the original oil/water mixture and the collected water after one time separation, respectively. The separation efficiency of SCuF for five kinds of selected oil is above 99%. SCuF exhibits excellent oil/water separation performance.

To further study the function of $Cu_2O/CuO_{1-x/2}Cl_x$ shell of Cu-NPs for oil/water separation, we compared the performance of anodized Cu foam and SCuF. The as-prepared anodized Cu foam also owns excellent superhydrophilicity and under-water superoleophobicity (see Fig. S5). However, its oil/water separation performance is inferior to SCuF (see Fig. S6), which can be illustrated by the WCP. The higher WCP of SCuF is beneficial to repel the oil,[27, 30] thus results the superior oil/water separation performance. Furthermore, the SCuF with polar $Cu_2O/CuO_{1-x/2}Cl_x$ shell shows stable superhydrophilicity even after storing for 3 months (see Fig. 4a).

3.3.2 The properties of the SCuF for repeated use

Then we analyzed the properties of the SCuF for repeated use, in which the oil model is hexane. The SCuF was rinsed by using deionized water for three times before the next test. As shown in Fig. 6a, the hexane content in separated water is about 1.6 ppm with little degeneration of oil/water separation performance even after 30 cycles, which shows highly stability. What's more, the poly-porous structue composed of hierarchical Cu-NPs remains the same (see Fig. 6b-c). This SCuF has great potential in real world applications.

3.3.3 The anti-corrosive properties of SCuF

Anti-corrosive property of membrane is a key factor for oil/water separation. For the real world applications, a good anti-corrosive property means that the membrane can operate continuously without degeneration of efficiency even in corrosive oil-containing wastewater. Recently, anti-corrosive membranes have been reported, in which the meshes were coated by organic,[61] inorganic-organic mixture,[62] polymer,[63] metals[64, 65] with nanostructures etc. to repel strong corrosive liquids. The SCuF can also bear corrosive liquids because of the metal Cu matrix.

The anti-corrosive properties of the SCuF were analyzed in solution with varied pH values. As shown in Fig. 7a, the OCA almost remains the same as the pH value varies from 1 to 14. Moreover, we also carried out the anti-corrosive experiments in 1 M HCl, 10 wt% NaCl and 1 M NaOH solution.[64] Fig. 7b shows the figure of OCA plotted against the immersed time in solutions, it is noticed that the OCA also remains stable for each case. However, the OCA in 1 M NaOH is smaller than other two cases, which is mainly due to the weaker interaction between the nucleophilic NaOH solution and the electron-rich $Cu_2O/CuO_{1-x/2}Cl_x$ shell of Cu-NPs according to Lewis's theory of valency, resulting in a more wafery solution layer between SCuF and oil-droplet as well as a smaller OCA for 1 M NaOH solution. Although the SCuF exhibits inferior under-water superoleophobicity in NaOH solution, the OCAs are larger than 150° for all cases. In other words, the SCuF shows well anti-corrosive properties for strong acidic, alkaline and salt solution. From Fig. 7c, we can see the residual hexane content in separated corrosive solution is about 2 – 3 ppm, and the separation efficiency is larger than 98.7% even for the 1 M NaOH solution. As is noticed that the separation efficiency for corrosive solutions is degenrated slightly when compared to

the hexane/water separation efficiency, which may be owing to the degraded under-water superoleophobicity (see Fig. 7b).

In order to illustrate the inherent anti-corrosive mechanism, we analysed the concentration of Cu ions (Cu^{2+} and Cu^{+}) in the corrosive solutions, for which 50 mg SCuF was immersed in 20 ml solution for 2 h and 10 h, respectively, to obtain the solution samples (see Fig. 7e). Fig. 7d shows the precipitation reactions of solution (after SCuF immersed for 2 h) by adding NaOH solution, the visual precipitation was only generated in 1 M HCl solution, indicating that the SCuF, especially the $Cu_2O/CuO_{1-x/2}Cl_x$ shell of Cu-NPs, was dissolved partly. The grass-green precipitation may be composed of blue $Cu(OH)_2$ and brick-red Cu_2O, then the precipitation turned into black CuO after aging for 2 h under air atmosphere. The concentration of Cu ions in the rest of solutions is so low that visual precipitation can not be generated. From Fig. 7f, it is noticed that the concentration of Cu ions in 10 wt% NaCl and 1 M NaOH solution is lower than 10 mg L^{-1}, meaning that the SCuF can resist this two corrosive liquids with the unaltered morphologies even immersed for 10 h (see Fig. S7). However, the concentration of Cu ions in 1 M HCl is higher than 500 mg L^{-1}, meaning that one fifth of the SCuF was dissolved in the solution, the SCuF with hierarchical nanoparticles turned into hierarchical pores structures. Fortunately, the amount of dissolved Cu just increased by 14% from 2 h to 10 h, in other words, the Cu foam with hierarchical pores structure is stable relatively in 1 M HCl on account of its Cu matrix. In 2015, Zhang et al.[29] reported an anti-corrosive membrane coated by Cu nanostructures for oil/water separation, the separation efficiency is above 99%, Cu nanostructures can act as active components for effective oil/water separation. Although the $Cu_2O/CuO_{1-x/2}Cl_x$ shell of SCuF is damaged, Cu foam with hierarchical pores structures also exhibits remarkable oil/corrosive solution separation perforemance, the separation efficiency is above 99% for hexane/1 M HCl mixture separation (see Fig. 7c).

4. Conclusions

In summary, we synthesized superhydrophilic Cu foam (SCuF) composed of oxy-chloridized hierarchical nanoparticles with metal Cu core and $Cu_2O/CuO_{1-x/2}Cl_x$ shell via the combination of anodization, HCl etching and calcination, in which the Cl-terminated groups were formed at the surface of Cu-NPs in the form of -O-Cu-Cl or even -Cu-Cl. This SCuF shows ultrahigh water permeability (5 µl water-droplet permeating within 9 ms) and remarkable oil/water separation performance (separation efficiency > 99%). Moreover, the properties of SCuF for repeated use and anti-corrosion are excellent. Due to the greatly enhanced specific surface area and active sites, it has potential applications in catalysis,[23] hydrogen evolution reaction,[66] electrode materials,[12] and many other environmental protection and energy fields.

We highlight our present work in the following four main aspects: Firstly, it is the first attempt to synthesize intrinsic SCuF for effective oil/water separation to the best of our knowledge. Secondly, this oxy-chloridized SCuF is easy to recycle and stable either in water or corrosive solutions. Thirdly, the specific surface area of SCuF is greatly enhanced because of the existence of surface hierarchical nanoparticles when compared to original Cu foam or Cu foam coated by functional substances, which is beneficial to lots of applications like catalysis, gas absorption, etc.. Fourthly, due to its layer-by-layer structure, it can endure much more scratch or friction cycles than those meshes coated by superhydrophilic substances theoretically. Becase if the superhydrophilic nanostructures in the top layer were broken, the inner layer can act as the active constituent for continuous applications.

Acknowledgements

This work was supported by Guangdong natural science foundation under Grant No.2014A030312009NSFC.

Notes and references

1. X. Zheng, H. Lee, T. H. Weisgraber, M. Shusteff, J. DeOtte, E. B. Duoss, J. D. Kuntz, M. M. Biener, Q. Ge, J. A. Jackson, S. O. Kucheyev, N. X. Fang and C. M. Spadaccini, *Science*, 2014, **344**, 1373-1377.
2. B. C. Tappan, M. H. Huynh, M. A. Hiskey, D. E. Chavez, E. P. Luther, J. T. Mang and S. F. Son, *J. Am. Chem. Soc.*, 2006, **128**, 6589-6594.
3. J. Zhang and C. M. Li, *Chem. Soc. Rev.*, 2012, **41**, 7016-7031.
4. M. Grden, M. Alsabet and G. Jerkiewicz, *ACS Appl. Mater. Interfaces*, 2012, **4**, 3012-3021.
5. X. Lin, F. Lu, Y. Chen, N. Liu, Y. Cao, L. Xu, W. Zhang and L. Feng, *Chem. Commun.*, 2015, **51**, 16237-16240.
6. M. Zeng and Y. Li, *J. Mater. Chem. A*, 2015, **3**, 14942-14962.
7. H. Jing-Fang and L. Bo-Tsuen, *Analyst*, 2009, **134**, 2306-2313.
8. Q. An, Y. Zhang, K. Lv, X. Luan, Q. Zhang and F. Shi, *Nanoscale*, 2015, **7**, 4553-4558.
9. L. Li, Z. Liu, Q. Zhang, C. Meng, T. Zhang and J. Zhai, *J. Mater. Chem. A*, 2015, **3**, 1279-1286.
10. J. Biener, A. Wittstock, L. A. Zepeda-Ruiz, M. M. Biener, V. Zielasek, D. Kramer, R. N. Viswanath, J. Weissmuller, M. Baumer and A. V. Hamza, *Nat. Mater.*, 2009, **8**, 47-51.
11. S. Cai, D. Zhang, L. Shi, J. Xu, L. Zhang, L. Huang, H. Li and J. Zhang, *Nanoscale*, 2014, **6**, 7346-7353.
12. M. S. Park, N. J. Lee, S. W. Lee, K. J. Kim, D. J. Oh and Y. J. Kim, *ACS Appl. Mater. Interfaces*, 2014, **6**, 10729-10735.
13. J. Song, Y. Lu, J. Luo, S. Huang, L. Wang, W. Xu and I. P. Parkin, *Adv. Mater. Interfaces*, 2015, **2**, 1500350.
14. Y. Hu, H. Lian, L. Zhou and G. Li, *Anal. Chem.*, 2015, **87**, 406-412.
15. H. Choi, O. H. Kim, M. Kim, H. Choe, Y. H. Cho and Y. E. Sung, *ACS Appl. Mater. Interfaces*, 2014, **6**, 7665-7671.
16. X. Ke, Y. Xu, C. Yu, J. Zhao, G. Cui, D. Higgins, Z. Chen, Q. Li, H. Xu and G. Wu, *J. Mater. Chem. A*, 2014, **2**, 16474-16479.
17. N. Chen and Q. Pan, *ACS Nano*, 2013, **7**, 6875-6883.
18. J. Zhang and C. M. Li, *Chem. Soc. Rev.*, 2012, **41**, 7016-7031.
19. C. Dong, H. Zhong, T. Kou, J. Frenzel, G. Eggeler and Z. Zhang, *ACS Appl. Mater. Interfaces*, 2015, **7**, 20215-20223.
20. Z. Li, Y. Chen, Y. Xin and Z. Zhang, *Sci. Rep.*, 2015, **5**, 16115.
21. Y. Lu, X. Liu, K. Qiu, J. Cheng, W. Wang, H. Yan, C. Tang, J. K. Kim and Y. Luo, *ACS Appl. Mater. Interfaces*, 2015, **7**, 9682-9690.
22. R. S. Dey, H. A. Hjuler and Q. Chi, *J. Mater. Chem. A*, 2015, **3**, 6324-6329.

23. D. DeCiccio, S. T. Ahn, S. Sen, F. Schunk, G. T. R. Palmore and C. Rose-Petruck, *Electrochem. Commun.*, 2015, **52**, 13-16.
24. Y. Shouguang, D. Jiangwei, S. Dong, L. Sheng and L. Jian, *Mater. Res. Innov.*, 2015, **19**, S5-617-S5-622.
25. F. Stergioudi, E. Kaprara, K. Simeonidis, D. Sagris, M. Mitrakas, G. Vourlias and N. Michailidis, *Mater. Design*, 2015, **87**, 287-294.
26. M. R. Mahmoud and N. K. Lazaridis, *Sep. Sci. Technol.*, 2015, **50**, 1421-1432.
27. Z. Xue, S. Wang, L. Lin, L. Chen, M. Liu, L. Feng and L. Jiang, *Adv. Mater.*, 2011, **23**, 4270-4273.
28. A. K. Kota, G. Kwon, W. Choi, J. M. Mabry and A. Tuteja, *Nat. Commun.*, 2012, **3**, 1025.
29. E. Zhang, Z. Cheng, T. Lv, Y. Qian and Y. Liu, *J. Mater. Chem. A*, 2015, **3**, 13411-13417.
30. F. Zhang, W. B. Zhang, Z. Shi, D. Wang, J. Jin and L. Jiang, *Adv. Mater.*, 2013, **25**, 4192-4198.
31. J. Li, L. Yan, H. Li, W. Li, F. Zha and Z. Lei, *J. Mater. Chem. A*, 2015, **3**, 14696-14702.
32. L. Zhang, Y. Zhong, D. Cha and P. Wang, *Sci. Rep.*, 2013, **3**, 2326.
33. M. A. Gondal, M. S. Sadullah, M. A. Dastageer, G. H. McKinley, D. Panchanathan and K. K. Varanasi, *ACS Appl. Mater. Interfaces*, 2014, **6**, 13422-13429.
34. X. Lin, F. Lu, Y. Chen, N. Liu, Y. Cao, L. Xu, Y. Wei and L. Feng, *ACS Appl. Mater. Interfaces*, 2015, **7**, 8108-8113.
35. Q. Wen, J. Di, L. Jiang, J. Yu and R. Xu, *Chem. Sci.*, 2013, **4**, 591-595.
36. Z.-Y. Luo, K.-X. Chen, Y.-Q. Wang, J.-H. Wang, D.-C. Mo and S.-S. Lyu, *J. Phys. Chem. C*, 2016, DOI: 10.1021/acs.jpcc.6b03940.
37. S. Jeong-Yun, Z. Xuanhe, W. R. K. Illeperuma, C. Ovijit, O. Kyu Hwan, D. J. Mooney, J. J. Vlassak and S. Zhigang, *Nature*, 2012, **489**, 133-136.
38. X. Gao, J. Zhou, R. Du, Z. Xie, S. Deng, R. Liu, Z. Liu and J. Zhang, *Adv. Mater.*, 2016, **28**, 168-173.
39. D. Zang, C. Wu, R. Zhu, W. Zhang, X. Yu and Y. Zhang, *Chem. Commun.*, 2013, **49**, 8410-8412.
40. Z.-Y. Luo, D.-C. Mo and S.-S. Lu, *J. Mater. Sci.*, 2014, **49**, 6742-6749.
41. S. Yu, B. Liu, Q. Wang, Y. Gao, Y. Shi, X. Feng, X. An, L. Liu and J. Zhang, *ACS Appl. Mater. Interfaces*, 2014, **6**, 10283-10295.
42. H. G. Yang, C. H. Sun, S. Z. Qiao, J. Zou, G. Liu, S. C. Smith, H. M. Cheng and G. Q. Lu, *Nature*, 2008, **453**, 638-641.
43. Y. Tian and L. Jiang, *Nat. Mate.r*, 2013, **12**, 291-292.
44. H. Bellanger, T. Darmanin, E. Taffin de Givenchy and F. Guittard, *Chem. Rev.*, 2014, **114**, 2694-2716.
45. A. V. Nikam, A. Arulkashmir, K. Krishnamoorthy, A. A. Kulkarni and B. L. V. Prasad, *Cryst. Growth Des.*, 2014, **14**, 4329-4334.
46. J. Y. Kim, J. A. Rodriguez, J. C. Hanson, A. I. Frenkel and P. L. Lee, *J. Am. Chem. Soc.*, 2003, **34**, 10684-10692.
47. T. P. Chopra, R. C. Longo, K. Cho, M. D. Halls, P. Thissen and Y. J. Chabal, *Chem. Mater.*, 2015, **27**, 6268-6281.
48. P. Chatterjee and S. Hazra, *J. Phys. Chem. C*, 2014, **118**, 11350-11356.
49. L. Yao and J. He, *Langmuir*, 2013, **29**, 3089-3096.
50. Z.-Y Luo, K.-X. Chen, D.-C. Mo and S.-S. Lyu, *J. Phys. Chem. C*, 2016, **120**, 11882-11888.
51. D. A. Svintsitskiy, T. Y. Kardash, O. A. Stonkus, E. M. Slavinskaya, A. I. Stadnichenko, S. V. Koscheev, A. P. Chupakhin and A. I. Boronin, *J. Phys. Chem. C*, 2013, **117**, 14588-14599.
52. L. Zhang, D. Jing, L. Guo and X. Yao, *ACS Sustainable Chem. Eng.*, 2014, **2**, 1446-1452.
53. M. Kawasaki, *J. Phys. Chem. C*, 2011, **115**, 5165-5173.
54. W. T. Yao, S. H. Yu, Y. Zhou, J. Jiang, Q. S. Wu, L. Zhang and J. Jiang, *J. Phys. Chem. B*, 2005, **109**, 14011-14016.
55. A. Chaudhary and H. C. Barshilia, *J. Phys. Chem. C*, 2011, **115**, 18213-18220.
56. J. Yu, J. Low, W. Xiao, P. Zhou and M. Jaroniec, *J. Am. Chem. Soc.*, 2014, **136**, 8839-8842.
57. H. Xu and L. Zhang, *J. Phys. Chem. C*, 2010, **114**, 11534-11541.
58. X. Zheng, Z. Guo, D. Tian, X. Zhang, W. Li and L. Jiang, *ACS Appl. Mater. Interfaces*, 2015, **7**, 4336-4343.
59. L. Wang, Y. Zhao, J. Wang, X. Hong, J. Zhai, L. Jiang and F. Wang, *Appl. Surf. Sci.*, 2009, **255**, 4944-4949.
60. M. Liu, S. Wang, Z. Wei, Y. Song and L. Jiang, *Adv. Mater.*, 2009, **21**, 665-669.
61. J. Li, D. Li, Y. Yang, J. Li, F. Zha and Z. Lei, *Green Chem.*, 2016, **18**, 541-549.
62. J. Li, R. Kang, X. Tang, H. She, Y. Yang and F. Zha, *Nanoscale*, 2016, **8**, 7638-7645.
63. J. Li, L. Yan, H. Li, J. Li, F. Zha and Z. Lei, *RSC Adv.*, 2015, **5**, 53802-53808.
64. E. Zhang, Z. Cheng, T. Lv, Y. Qian and Y. Liu, *J. Mater. Chem. A*, 2015, **3**, 13411-13417.
65. L. Liu, C. Chen, S. Yang, H. Xie, M. Gong and X. Xu, *Phys. Chem. Chem. Phys.*, 2016, **18**, 1317-1325.
66. J. Zhang, M. D. Baro, E. Pellicer and J. Sort, *Nanoscale*, 2014, **6**, 12490-12499.

Table of contents (TOC) for Journal of Material Chemistry A:

Hierarchical nanoparticles-induced superhydrophilic and under-water superoleophobic Cu foam with ultrahigh water permeability for effective oil/water separation

Zhi-Yong Luo, Kai-Xuan Chen, Jun-Hui Wang, Dong-Chuan Mo* and Shu-Shen Lyu*

School of Chemical Engineering and Technology, Sun Yat-sen University, Guangzhou 510275, China.

E-mail: modongch@mail.sysu.edu.cn and lvshsh@mail.sysu.edu.cn; Fax: +86-020-84112150

Table of contents (TOC)

Superhydrophilic Cu foam (SCuF) that consists of oxy-chloridized hierarchical nanoparticles is first synthesized for effective oil/water separation.